

Document downloaded from:

<http://hdl.handle.net/10251/75269>

This paper must be cited as:

Fortunati, E.; Cano Embuena, Al.; Cháfer Nácher, MT.; González Martínez, MC.; Chiralt A.; Kenny, JM. (2015). Effect of cellulose nanocrystals on the properties of pea starch/poly(vinyl alcohol) blend films. *Journal of Materials Science*. 50(21):6979-6992. doi:10.1007/s10853-015-9249-9.



The final publication is available at

<https://dx.doi.org/10.1007/s10853-015-9249-9>

Copyright Springer Verlag (Germany)

Additional Information

1 **Effect of cellulose nanocrystals on the properties of pea starch- poly(vinyl**  
2 **alcohol) blend films.**

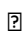
3 **A. Cano<sup>a</sup>, E. Fortunati<sup>b\*</sup>, M. Cháfer<sup>a</sup>, C. González-Martínez<sup>a</sup>, A. Chiralt<sup>a</sup>, J.M.**  
4 **Kenny<sup>b,c</sup>**

5 <sup>a</sup>Instituto de Ingeniería de Alimentos para el Desarrollo, Universitat Politècnica de  
6 València. Camino de Vera s/n 48022 Valencia, Spain.

7 <sup>b</sup>Materials Engineering Centre, UdR INSTM, University of Perugia, Strada di Pentima 4,  
8 05100 Terni, Italy.

9 <sup>c</sup>Institute of Polymer Science and Technology, CSIC, Juan de la Cierva 3, 28006  
10 Madrid, Spain.

11

12 \*Corresponding Author. Tel.: +39-0744-492921 Fax: +39-0744-492950, Strada di  
13 Pentima, 4, 05100, Terni, e-mail address:  HYPERLINK

14 "mailto:elena.fortunati@unipg.it"  elena.fortunati@unipg.it  (Elena Fortunati)

15

16

17 **Abstract**

18 Incorporation of cellulose nanocrystals (CNCs) to pea starch-poly(vinyl alcohol) (PVA)  
19 (1:2 ratio) blend films was carried out in order to improve their mechanical and barrier  
20 properties and film stability throughout storage, thus overcoming some drawbacks of  
21 starch based films. Different ratios (1, 3 and 5 %) of CNC were used and structural,  
22 thermal and physical (barrier, mechanical and optical) properties were analysed in  
23 comparison to the control film without CNC. Incorporation of CNC enhanced phase  
24 separation of polymers in two layers. The upper PVA rich phase contained lumps of  
25 starch which emerged from the film surface, thus reducing the film gloss. CNC were  
26 dispersed in both polymeric phases as aggregates, whose size increased with the CNC  
27 ratio rise. CNC addition did not implied changes in water vapour barrier of the films, but  
28 they became slightly stiffer and more stretchable, while crystallization of PVA was  
29 partially inhibited.

30

31

32 **Keywords:** microstructure, mechanical properties, nanocomposites, optical properties,  
33 phase transitions, water vapour permeability.

34

## 35 **Introduction**

36 The growing interest in environmentally-friendly materials has promoted research into  
37 the development of biodegradable polymers as an alternative to non-biodegradable  
38 synthetic petroleum-derived polymers [1, 2]. In response to the consumer requirements  
39 for safer and environmentally friendly packaging materials, the combination of  
40 biodegradable polymers with bio-based additives has also been analysed to improve  
41 the properties of these materials [3]. In this sense, bio-resources obtained from  
42 agricultural-related industries have received special attention. Crops fibre components  
43 provide a wide range of opportunities for developing new applications in different  
44 industrial sectors such as packaging, building, automotive and aerospace industries,  
45 electronics, etc. [4].

46 In the development of packaging materials for food applications, polysaccharides, such  
47 as starch, cellulose and their derivatives have commonly been used as film-forming  
48 compounds [5]. Cellulose is the most abundant renewable natural polymer resource  
49 available in the biosphere [6-8]. It is well known that when cellulose fibres are  
50 subjected to acid hydrolysis, the fibres yield defect-free, rod-like crystalline residues [6].  
51 The use of cellulose nanocrystals (CNCs) as fillers in packaging materials has been  
52 studied not only because of their interesting physical and chemical properties but also  
53 due to their inherent renewability, sustainability and abundance. The most common  
54 sources of these nanocrystals include cellulose fibres from cotton, hemp, flax,  
55 microcrystalline cellulose, bacterial cellulose [6, 7, 9, 10]. The production of cellulose  
56 nanocrystals consists of subjecting pure cellulose material to strong acid hydrolysis  
57 under controlled conditions such as temperature, agitation and time, which determine  
58 the structure and characteristics of the crystals. Cellulose nanocrystals are used as a  
59 reinforcement material due to their large specific surface area ( $150 \text{ m}^2\text{g}^{-1}$ ) [11], surface  
60 energy [12] and very high elastic modulus (about 150 GPa) [13]. Moreover, their low  
61 density, about  $1.566 \text{ g cm}^{-3}$  [10], biocompatibility, biodegradability, low energy  
62 consumption in manufacturing, and low cost represent remarkable advantages of

63 cellulose nanocrystals [10, 12, 14, 15] in comparison to others nanomaterials such as  
64 nanoclays, SiO<sub>2</sub> and Au nanoparticles for elaboration of low cost nanocomposites. All  
65 of this makes cellulose nanostructures to be advantageous bio-based edible additives,  
66 which are able to enhance the bio-polymer performance, in terms of the mechanical,  
67 thermal and barrier properties [2, 8]. However, cellulose nanocrystals have some  
68 drawbacks, such as the difficulty to disperse homogenously in the polymer matrix [14],  
69 as a result of their agglomeration into flakes during film formation. Due to the  
70 hydrophilic character of cellulose nanocrystals, the main technique employed to  
71 transfer them from an aqueous dispersion into an organic polymer has been the  
72 casting-evaporation process [6].

73 Biopolymer nanocomposites are the result of the combination of biopolymers and  
74 nanoparticles of inorganic/organic fillers [15]. Cellulose nanocrystals have been  
75 incorporated into a wide variety of biopolymer matrices including (poly)caprolactone  
76 [16], carboxymethyl cellulose [17], (poly)vinyl alcohol [7, 8, 10, 15], (poly)lactic acid [9,  
77 14], chitosan [18], starch [5, 19] and biopolymer blends, like poly(lactic acid)-  
78 poly(hydroxybutyrate) [20, 21]. In general, the hydrophilic nature of both biopolymer  
79 and nanocrystals leads to excellent interfacial compatibility, resulting in enhanced  
80 mechanical and thermal properties of the composite material [5, 15].

81 The use of starch as a biopolymer matrix in combination with other polymers to reduce  
82 the starch film drawbacks (poor mechanical and water vapour barrier properties) has  
83 been explored by different authors [22, 23]. The incorporation of PVA into gelatinized  
84 pea starch matrices implied the formation of interpenetrated polymer networks. In fact,  
85 the blend films showed beneficial effects on the mechanical properties of the films,  
86 these becoming much more extensible and stable during storage, and on water barrier  
87 properties [24]. Different studies into starch-PVA blends have been carried out,  
88 focusing on their biodegradability [25, 26] and the effect of the incorporation of different  
89 additives to the blends. The effect of adding citric acid [26], glutaraldehyde [27], urea  
90 [28], calcium chloride [29], or nanoparticles like nano-sized poly(methyl methacrylate-

91 co-acrylamide) particles [30] on PVA-starch blend properties has been analysed for  
92 different aims (compatibility enhancement or development of biomedical and packaging  
93 materials). Nevertheless, no studies have been found into the effect of cellulose  
94 nanocrystals on the properties of pea starch-PVA blend films.

95 The aim of the present work was to study the effect of incorporating cellulose  
96 nanocrystals into pea starch-PVA blend films in terms of their nano- and micro-  
97 structure, thermal behaviour and physical properties at different ageing times.

98

## 99 **2. Materials and Methods**

### 100 2.1 Materials

101 Pea starch (S) was purchased from Roquette Laisa España S.A. (Benifaó, Valencia,  
102 Spain), poly(vinyl alcohol) (PVA) ( $M_w$ : 89.000-98.000, hydrolysed, +99%, viscosity:  
103 11.6-15.4 cP, 4% in H<sub>2</sub>O at 20 °C), microcrystalline cellulose (MCC) (powder, 15 - 20  
104  $\mu$ m) were from Sigma Aldrich Química S.L. (Madrid, Spain). Glycerol and magnesium  
105 nitrate-6-hydrate ( $Mn(NO_3)_2$ ) were supplied by Panreac Química S.A. (Castellar de  
106 Vallès, Barcelona, Spain). Sulphuric acid, ion resin (Dowex Marathon MR-3 hydrogen  
107 and hydroxide), Whatman 541 filter paper and NaOH were also purchased from Sigma  
108 Aldrich Química S.L. (Milan, Italy).

109

### 110 2.2. Extraction of Cellulose nanocrystals (CNC).

111 A suspension of cellulose nanocrystals (CNC) was prepared from microcrystalline  
112 cellulose (MCC) by hydrolysis using sulphuric acid, 64 % (wt/wt) at 45 °C for 30 min, as  
113 previously reported by Cranston and Gray [31] and Fortunati [9]. Immediately following  
114 the acid hydrolysis, the suspension was diluted 20 fold with deionized water and  
115 maintained at rest overnight. Afterwards, the dispersion was centrifuged at 4,500 rpm  
116 for 20 min to separate the cellulose crystals. The precipitate was dialyzed against  
117 deionized water for 5 days and then neutralized with mixed bed ion resin for 48 h.

118 Afterwards, the suspension was filtered through filter paper. The CNC filtrate was  
119 neutralized by adding 1.0 % (v/v) of 0.25 M NaOH. Finally, the CNC dispersion was  
120 homogenized by ultrasonic treatment, using a tip sonicator (Vibracell, 750 Sonics &  
121 Materials, Inc., Newton, USA) for 10 min in an ice bath. The dry matter content of the  
122 CNC dispersion was determined by the drying oven method [32], giving  $11.1 \pm 0.2$  %.  
123 This value was a little low compared with that reported by other authors [21]. CNC  
124 obtained nano-crystals showed dimensions ranging from 100 to 200 nm in length and 5  
125 to 10 nm in width, according to FSEM observations [10].

126

### 127 2.3. Preparation of films

128 Films were obtained by casting from film forming dispersions (FFDs). Starch (1 %w/w)  
129 was dispersed in an aqueous solution at 90 °C for 30 min with continuous stirring to  
130 induce starch gelatinization. Thereafter, the dispersion was homogenized using a rotor-  
131 stator homogenizer (Ultraturrax D125, Janke and Kunkel, Germany) at 13,500 rpm for  
132 1 min and 20,500 rpm for 3 min. Immediately following the starch gelatinization, PVA  
133 was dispersed in the aqueous solution in a S-PVA ratio of 1:2 (w/w), and maintained at  
134 90 °C for 30 min until complete dissolution. When the dispersion was cooled, 0.25 g of  
135 glycerol per g of starch was added on the basis of previous studies [33]. This FFD was  
136 used to obtain the control films. Cellulose nanocrystal dispersion was homogenized  
137 with the polymer FFDs by means of a tip sonicator for 4 min in ice bath. Different CNC  
138 mass ratios were considered: 0, 1, 3 and 5 g of CNC per 100 g of total polymers  
139 (sample codes: C, 1 %, 3 % and 5 %, respectively), considering the dry weight of CNC  
140 and polymers.

141 To obtain the films, the FFDs were poured into Petri dishes, in a proper amount to  
142 provide a surface density of solids of  $145 \text{ g m}^{-2}$ . Films were dried at 40 °C in a  
143 convection oven for 48 h and afterwards, peeled off the casting surface and  
144 conditioned at 53 % RH, using magnesium nitrate-6-hydrate ( $\text{Mn}(\text{NO}_3)_2$ ) saturated  
145 solution at room temperature ( $\approx 25$  °C) until further analysis. The film thickness was

146 measured at six random positions with a calliper (MicrometerStarrett) to the nearest  
147 0.001 mm.

148

## 149 2.4. Characterization of films

### 150 2.4.1. Microstructure

151 Microstructural analysis of films was carried out using both a field emission scanning  
152 electron microscope (FESEM) (Supra™ 25-Zeiss, Germany) and an atomic force  
153 microscope (AFM) (Multimode 8, Bruker AXS, Inc. Santa Barbara, California, USA),  
154 with a NanoScope® V controller electronics. To this end, two replicates per formulation  
155 were observed. FESEM observations were carried out on the film surface and on their  
156 cross section. To prepare the cross section samples, films were frozen in liquid  
157 nitrogen and cryofractured. Afterwards, samples were gold coated, and observed using  
158 an accelerating voltage of 2 and 5 kV, for the surface and cross-section observations,  
159 respectively.

160 The surface morphology was also analysed using AFM. The resulting data were  
161 transformed into a 2D image. Measurements were taken from 50 x 50  $\mu\text{m}$  and 3 x 3  $\mu\text{m}$   
162 areas of the film surface, using the phase imaging mode.

163 AFM with the peak force QNM (Quantitative NanoMechanics) mode was also used to  
164 analyse the film surface nanostructure. Measurements were taken from 20 x 20  $\mu\text{m}$   
165 areas of the film surface and the resulting data were transformed into a 2D image  
166 (DMT modulus map).

167

### 168 2.4.2. Fourier Transform Infrared (FTIR) spectroscopy

169 FTIR spectra of the films were obtained by a Jasco FT-IR 615 spectrometer, (Easton  
170 MD, USA) in transmission mode, in the range of 400-4000  $\text{cm}^{-1}$ . A few drops of  
171 different film forming dispersions were cast on silicon plates, after which they were  
172 dried and measured. Each sample was characterized in duplicate.

173



174 2.4.3. Thermogravimetric analysis

175 Thermal weight loss (TG) and its derivate (DTG) of film samples vs. temperature were  
176 obtained using a thermogravimetric analyzer (Seiko Exstar 6300, Italy). In the test,  
177 samples were heated from 30 °C to 600 °C at 10 °C min<sup>-1</sup>, using a nitrogen flow. Prior  
178 to the analyses, samples were conditioned for 1 week. Thermal degradation  
179 temperatures (the maximum of the DTG curves (T<sub>mp</sub>) and secondary degradation  
180 temperature peak (T<sub>p</sub>)) were obtained. Measurements were taken in triplicate.

181

182 2.4.4. Differential scanning calorimetry

183 Differential scanning calorimeter (DSC) (TA Instrument, Q200, USA) was used to  
184 analyse phase transitions in the films as a function of the temperature. Measurements  
185 were carried out in triplicate under nitrogen flow in the temperature range -25 to 230  
186 °C, at 10 °C min<sup>-1</sup>, by performing three scans: First, samples were heated from room  
187 temperature to 230 °C and maintained for 5 min at 230 °C. Then, samples were cooled  
188 down to - 25 °C and heated again until 230 °C. Data were recorded both during the  
189 cooling and second heating steps. From thermograms of the cooling step, the  
190 crystallization temperatures (T<sub>c</sub>) and enthalpy (ΔH<sub>c</sub>) values were obtained. From the  
191 second heating step, glass transition temperature (T<sub>g</sub>), melting temperature (T<sub>m</sub>) and  
192 melting enthalpy (ΔH<sub>m</sub>) values were obtained. Prior to the analyses, samples were  
193 conditioned for 1 week.

194 The crystallinity degree of PVA was calculated as shown in equation 1:

195 
$$X = \frac{1}{X_{PVA}} \left[ \frac{\Delta H}{\Delta H_0} \right] 100 \quad (1)$$

196 Where ΔH, is the melting enthalpy of the sample (expressed in J g<sup>-1</sup> PVA), ΔH<sub>0</sub>, the  
197 melting enthalpy of a 100% crystalline PVA sample (161.6 J.g<sup>-1</sup> [34]) and X<sub>PVA</sub>, the  
198 mass fraction of PVA in the film.

199

#### 200 2.4.5. Moisture content

201 Film moisture content (MC) was analysed by drying the film samples in a vacuum oven  
202 at 60 °C for 24 h. Later on, the pre-dried samples were placed in desiccators containing  
203 P<sub>2</sub>O<sub>5</sub> until reaching a constant weight. Five replicates per film formulation for one and  
204 five weeks were analysed.

205

#### 206 2.4.6. Water vapour permeability (WVP)

207 Water vapour permeability (WVP) was evaluated in films equilibrated for 1 and 5  
208 weeks, following the gravimetric method ASTM E96-95 [35] by using Payne  
209 permeability cups (Payne, elcometer SPRL, Hermelle/sd Argenteau, Belgium) of 3.5  
210 cm diameter. Deionised water was used inside the testing cup to achieve 100 % RH on  
211 one side of the film, while an oversaturated magnesium nitrate solution was used to  
212 control the RH on the other side of the film. A fan placed on the top of the cup was  
213 used to reduce resistance to water vapour transport. Water vapour transmission rate  
214 measurements (WVTR) were performed at 25 °C. To calculate WVTR, the slopes in  
215 the steady state period of the weight loss vs. time curves were determined by linear  
216 regression. WVP was calculated according to [36]. For each type of film, WVP  
217 measurements were taken in quadruplicate.

218

#### 219 2.4.7. Mechanical properties

220 Mechanical properties were measured using a Universal Test Machine (Digital Lloyd  
221 instrument, West Sussex, UK), following the UNI ISO 527-1 [37], by using 5 mm min<sup>-1</sup>  
222 and a load cell of 1.5 N. Equilibrated film samples (1 x 5 cm) for 1 and 5 weeks were  
223 mounted in the film-extension grips (A/TG model), which were set 20 mm apart. Stress-  
224 Hencky strain curves were obtained and the tensile strength at break (TS), percentage  
225 of elongation at break (ε) and elastic modulus (EM) were calculated. Measurements  
226 were taken at room temperature with eight replicates per formulation.

227

#### 228 2.4.8. Ultraviolet-visible spectrophotometry

229 Film samples equilibrated (1 x 1 cm) for 1 and 5 weeks were analysed by means of a  
230 UV–VIS spectrophotometer (Perkin Elmer Instruments, Lambda 35, Waltham, USA), by  
231 using a wavelength range between 250 and 1000 nm.

232

#### 233 2.4.9. Internal transmittance

234 Internal transmittance ( $T_i$ ) as a measure of the transparency of the films was  
235 determined through the surface reflectance spectra in a spectrophotometer CM-3600d  
236 (Minolta Co, Tokyo, Japan) with a 30 mm illuminated sample area by applying the  
237 Kubelka–Munk theory for multiple scattering to the reflection spectra, following the  
238 methodology described by Cano, et al. [36]. Measurements were taken in triplicate in  
239 films equilibrated for 1 and 5 weeks.

240

#### 241 2.4.10. Gloss

242 Gloss was measured using a flat surface gloss meter (Multi- Gloss 268, Minolta,  
243 Langenhagen, Germany) at an incidence angle of  $60^\circ$ , according to the ASTM standard  
244 D523 [38]. Prior to gloss measurements, films were conditioned for 1 and 5 weeks.  
245 Gloss measurements were performed in triplicate. Results were expressed as gloss  
246 units, relative to a highly polished surface of standard black glass with a value close to  
247 100.

248

#### 249 2.4.11. Overall migration

250 Overall migration tests in films conditioned for 1 week were carried out by following  
251 current legislation [39, 40]. Rectangular film strips of 20 cm<sup>2</sup> total area were immersed  
252 in a glass tube with 20 mL of food simulants (ethanol 10 % (v/v) -simulant A- (Sigma  
253 Aldrich Química S.L., Milan, Italy) and isooctane - simulant to D2- (Sigma Aldrich  
254 Química S.L., Milan, Italy)), keeping the established relation of 6 dm<sup>2</sup> kg<sup>-1</sup>. Samples in  
255 simulant A were kept in a controlled chamber at 40 °C for 10 days, while samples in

256 isooctane were kept at 20 °C for 2 days. After the incubation period, the films were  
257 removed and simulants were evaporated to dryness. Afterwards, the residue was  
258 weighed with  $\pm 0.001$  mg precision in order to determine the overall migration value in  
259  $\text{mg kg}^{-1}$  of simulant. For each sample, three determinations were carried out.

260

## 261 2.5. Statistical analysis

262 Results were analysed by analysis of variance (ANOVA), using the Statgraphics Plus  
263 5.1. Program (Manugistics Corp., Rockville, MD). To differentiate samples, Fisher's  
264 least significant difference (LSD) was used at the 95 % confidence level.

## 265 **3. Results and discussion**

### 266 3.1. Nano- and micro-structure of the films

267 Figures 1 and 2 show the FESEM micrographs of the surfaces and cross sections of  
268 the different films, respectively. Control films showed phase separation of starch and  
269 PVA due to the lack of polymer compatibility, according to what was previously  
270 observed by other authors [24, 41]. Surface of control films shows the formation of  
271 globular structures which can be attributed to domains of one of the polymeric phases  
272 dispersed in the continuous phase of the other. When CNC nanocrystals were  
273 incorporated into the film formulation, the surface concentration of dispersed domains  
274 increased, this being more marked for the highest CNC content (5 %).

275 The cross section micrographs of control films (Figure 2) showed two interpenetrated  
276 networks of both polymers where the crystalline zones of PVA can also be appreciated.

277 In films containing CNCs the formed two layers in the films are more clearly  
278 differentiated. The top phase corresponds to about one third of the film thickness,  
279 according to the ratio of starch to PVA, which suggest that starch rich phase mostly  
280 separated at the top of the films whereas PVA predominate in the down layer. The top  
281 layer generally shows a less smooth appearance, showing the coexistence of PVA  
282 dispersed domains in a more continuous starch matrix. Some of them emerged to the

283 film surface, as shown in the surface micrographs (Figure 1). The PVA rich phase also  
284 shows lumps of starch phase. Distribution of nanoparticles in the different phase  
285 cannot be clearly appreciated at the magnification level of micrographs, although the  
286 PVA phase shows a more granular aspect which could indicate that nanoparticles  
287 could be present in this phase to a greater extent. Micrographs at higher magnification  
288 allow us to appreciate this effect. For the highest ratio of CNCs (5 %), these appear  
289 distributed in both phases, thus modifying their general appearance. The aggregation  
290 of CNC in some film areas could be observed, which is due to their strong hydrogen  
291 bonding capacity. Khoshkava and Kamal [12] also reported that at higher CNC  
292 concentration CNC aggregation occurs to a great extent.

293 Figure 3 shows AFM images of control film and those containing CNC, obtained by  
294 using Phase Imaging mode derived from Tapping Mode. Raw data were converted into  
295 2D images and their scale is expressed as degrees. Phase Imaging allows to detect  
296 variations in composition, adhesion, friction, viscoelasticity and other properties in the  
297 material surface at nano-scale level, providing material property contrast. Surface of 50  
298  $\mu\text{m}^2$  of control films shows two different phases in agreement with that observed in the  
299 surface FESEM images. The dispersed phase in the control film corresponds to  
300 emerging PVA lumps in the starch continuous phase of the upper layer of the films.  
301 Nevertheless, the dispersed phase concentration at the film surface increased when  
302 CNC ratio rose in the formulation. Observations a higher magnification (areas of 3  $\mu\text{m}^2$ )  
303 were carried out on the continuous and dispersed surface phases to observe possible  
304 location of CNC at the film surface. These images are shown in Figure 3. For 1 % of  
305 CNC, no evidences of the nanocrystals in any phase are detected, probably due to  
306 their low ratio in film formulation. Nevertheless, at 3 % and 5 %, CNCs were observed  
307 in both, dispersed and continuous polymer phases. At 3 % of CNC, great aggregates of  
308 particles are present in the continuous phase (mean size 200 nm) whereas particles  
309 are better dispersed in the PVA dispersed phase. At 5 % CNCs, particle aggregation is  
310 more accused appearing as enlarged formations whose perimeter is completely

311 covered by flocculated nanocrystals. This formations appeared in both PVA and starch  
312 phases at the surface. As reported by Arrieta et al. [21] the greater the CNC  
313 concentration, the higher the aggregation level in the system.

314 Differences in the surface mechanical resistance were observed by means of AFM in  
315 Peak Force QNM mode (Figure 4). The maps of Log DMT modulus for control films  
316 revealed the two phases previously mentioned at surface level, but no great differences  
317 in mechanical resistance between both could be detected. In 1 % CNC film formulation,  
318 similar values of log DMT modulus to those of control films were observed, probably  
319 due to low concentration of CNC in the observed area, as deduced in phase imaging.  
320 The incorporation of 3 % and 5 % of CNC gave rise to much higher differences in the  
321 values of DMT modulus of a given surface, especially for 3 %. In this case, the hardest  
322 areas are particulate in shape, which agrees with the greater hardness of crystalline  
323 structure of dispersed CNC. At 5 %, a high proportion of very soft small areas can be  
324 observed, which can be attributed to voids left by the aggregates of CNC which  
325 probably are separated from the surface by the cantilever during the test, in part due to  
326 their big size, despite the images reveals good interfacial adhesion of CNC to the pea  
327 starch-PVA matrix.

328 Figure 5 shows FTIR spectra for control and nanocomposite films, showing the  
329 wavenumber values corresponding to the main peaks in each sample. The spectrum of  
330 the control film showed several characteristic peaks of stretching and bending  
331 vibrations of groups of starch and PVA chains. The broad band located between 3200-  
332 3600  $\text{cm}^{-1}$  corresponds to the stretching vibration mode of hydroxyl groups from the  
333 absorbed water and from the polymers themselves, [10, 42, 43]. The relative intensity  
334 of this band decreased when the ratio of CNC increased in the films. The peak at  
335 around 2940  $\text{cm}^{-1}$  is related with alkyl groups, C-H stretching [10, 43, 44] and it  
336 increased in intensity as the CNC ratio increased, which can be explained by the  
337 contribution of C-H vibration in the crystalline structures. The peak at 1645  $\text{cm}^{-1}$   
338 corresponds to the H-O-H group deformation [10] and it appears better resolved in

339 films with CNC. The peaks associated with the bending vibration mode of hydroxyl  
340 group appear at around  $1420\text{ cm}^{-1}$  and they show a slight displacement of 20 units with  
341 respect to the control film when CNC are present in the matrix, while an increase in  
342 intensity and resolution of this peak was observed when CNC ratio increased up to 3  
343 %. The stretching vibration of C-O in the C-C-O group and in the starch glucose ring  
344 corresponds to the peaks at  $1032$  and  $854\text{ cm}^{-1}$ , respectively [10]. These bands also  
345 suffered changes due to the presence of CNC in the films.

346 The addition of CNC, especially at 3 and 5 %, resulted in a slight reduction of the  
347 intensity of the -OH stretching band, a widening of band at  $2940\text{ cm}^{-1}$  due to C-H  
348 stretching, the appearance of an additional peak at  $1733\text{ cm}^{-1}$ , assigned to the C-C-O  
349 stretching, and changes in the peaks resolved between  $850$  and  $1670\text{ cm}^{-1}$ . In this  
350 sense, it is remarkable that the C-OH bending vibrations of alcohol groups present in  
351 cellulose appear at  $1100\text{ cm}^{-1}$  [10]. The slight changes introduced by CNC in the FTIR  
352 spectra of PVA-starch films suggest the interactions between hydroxyl groups (-OH) on  
353 the CNC surface and the -OH of the polymer blend chains, as proposed by other  
354 authors [50].

355

### 356 3.2. Thermal properties of the films

357 DSC and TGA measurements were used to study the thermal behaviour of the films, in  
358 order to know phase transitions and the thermal stability of the materials [45] as  
359 affected by the addition of CNC at different contents.

360 Table 1 shows the results obtained from the DSC analysis. The PVA crystallization  
361 pattern showed one secondary peak at about  $144\text{ }^{\circ}\text{C}$  and a main peak located around  
362  $201\text{ }^{\circ}\text{C}$ . Secondary peak appears at lower temperatures (supercooling) due to kinetic  
363 hindrances attributable to the low mobility of the polymer chain segments at the end of  
364 the crystallization process. The melting temperature ( $T_m$ ) of control films was  $227\text{ }^{\circ}\text{C}$ ,

365 without the split observed in crystallization. No significant effect of the CNC  
366 incorporation was observed in the  $T_m$  values, as previously found by Habbi et al. [6].  
367 Crystallization enthalpy (Table 1), expressed as  $J g^{-1}$  of PVA, showed a certain degree  
368 of variability and there were no significant differences among samples. The average  
369 value was  $70 J g^{-1}$  of PVA, slightly lower than the melting enthalpy value, which  
370 indicates that supercooling occurred during the cooling step. Values of melting  
371 enthalpy, expressed in  $J g^{-1}$  of PVA, reveal that PVA crystallization was partially  
372 inhibited by the presence of CNC, since the  $\Delta H_m$  value decreased as the CNC ratio in  
373 the films rose. In fact, the degree in crystallinity of PVA ( $X$  in Table 1) was reduced by  
374 about 50 %, with respect to the control film, when 5 % of CNC was added. However,  
375 Rescignano et al. [15] observed that the crystallinity increases slightly with the addition  
376 of cellulose nanocrystals in PVA films, although their reported values are much smaller  
377 (15 %) as compared with the obtained values in this study (close to 70 % in control  
378 film). The CNC inhibition effect in PVA crystallization is also deduced from the greater  
379 supercooling observed in the cooling scan for samples containing CNC.

380 Glass transition observed in the films must be assigned to the PVA phase bearing in  
381 mind the temperature range where it occurs, while this transition was not detected for  
382 the starch phase, due to its lower ratio in the film. Our previous studies [24] on PVA-  
383 starch blend films found the  $T_g$  values at  $124 \pm 2$  °C and at  $76 \pm 4$  °C, respectively for the  
384 starch and PVA phases.  $T_g$  values were taken from the heating step when  
385 crystallization of PVA is completed and the amorphous phase contains the non-  
386 crystallized fraction. In all cases, the values obtained in the cooling step were slightly  
387 lower, which indicates that the mean molecular weight of the amorphous fraction is  
388 lower when crystallization was not completed. Therefore, this would point to the fact  
389 that the longer chains crystallize prior to the shorter ones. The obtained  $T_g$  value of  
390 PVA in the control films was 79 °C, which was similar to that reported by other authors  
391 for PVA films [10, 15]. The incorporation of CNC to the films provoked a decrease of  
392 about 2 °C, which can be related with the partial inhibition of the PVA crystallization



393 (especially the shorter chains, as commented on above) and the subsequent decrease  
394 of the mean molecular weight of the amorphous PVA fraction. Other authors [6, 9, 15]  
395 did not found changes in the glass transition temperature of the polymer (PLA and  
396 PVA) when cellulose nanocrystals were incorporated to the matrix.

397 DSC analysis reveals that PVA crystallization was partially inhibited when CNC are  
398 present as filler in the blend films, this effect being more marked when they contain 5 %  
399 of nanocrystals. The lack of crystallization gave rise to a decrease in the T<sub>g</sub> of the  
400 amorphous phase which suggests that the shorter PVA chains remain in the  
401 amorphous phase.

402 Figure 6 shows the weight loss (TG curve) and its derivate (DTG curve) as a function of  
403 the temperature for control films and formulations containing cellulose nanocrystals.  
404 The temperatures for the main degradation steps of the films are summarized in Table  
405 1. For control films, three weight loss steps were observed. Similar multi-step weight  
406 loss behaviour was described for PVA films [7, 15] and for corn starch-PVA blend films  
407 obtained by casting [40]. The initial weight loss, up to about 90 °C, can be attributed to  
408 the loss of bonded water in the film [7, 8, 27] with total weight loss in this range of  
409 about 10 %. The second step, between 150-380 °C, is related to the main degradation  
410 process (peak temperature 347 °C), in which dehydration reactions, followed by  
411 polymer scission and decomposition, take place. Total weight loss in this range is  
412 about 70 %. Moreover, in this step the acetyl groups of PVA were transformed into  
413 acetic acid molecules and successive catalytic degradation of the main chain by in situ  
414 stripping at higher temperatures occurs [15, 46]. The third step takes place at between  
415 380 – 500 °C and it can be attributed to the degradation of the by-products generated  
416 by PVA during the thermal process [7, 23]. In previous studies, it was observed that in  
417 pea starch films only two weight loss steps occur: the loss of bonded water up to 100  
418 °C and the main degradation at 315 °C.

419 The addition of cellulose nanocrystals into the films led to a similar weight loss pattern  
420 to the control films, showing the three weight loss steps commented on above (Figure

421 6). There were no notable changes in the pattern of thermal degradation of  
422 nanocomposites or in the temperature of the main peaks (Table 1), except for films with  
423 5 % CNC, where a slight decrease in  $T_{mp}$  was observed. Likewise, the temperature of  
424 the secondary peak was slightly higher due to the influence of cellulose thermal  
425 behaviour [15].

426

### 427 3.3. Physical properties of the films

428 The analysis of the physical properties of studied films was carried out to know their  
429 barrier, optical and mechanical behaviour. Film thickness was  $98 \pm 8 \mu\text{m}$  for all  
430 formulations. Table 2 shows the water vapour permeability values (WVP) of the films at  
431  $25 \text{ }^\circ\text{C}$  and at a 53-100 % RH gradient, together with their equilibrium moisture content  
432 and optical properties after 1 and 5 storage weeks. After 1 week, the moisture content  
433 was slightly lower for samples containing 3 % and 5 % CNC, but their value increased  
434 throughout 5 storage weeks, reaching a similar value in all cases in the range 6-7 %.  
435 This suggests that CNC limit the moisturising rate till sample equilibration, despite the  
436 hydrophilic character of these nanoparticles [6, 10], probably due to the structural  
437 changes induced in the films and the increase in the tortuosity factor in the matrix  
438 associated with the presence of the dispersed nanoparticles.

439 The WVP values of the films must be as low as possible to efficiently limit the water  
440 vapour transfer when it is in contact with food systems [19]. Mean values of studied  
441 films ranged between  $3.1\text{-}3.6 \text{ g}\cdot\text{mm}\cdot\text{kPa}^{-1}\cdot\text{h}^{-1}\cdot\text{m}^{-2}$  and no notable differences are found  
442 among formulations or due to the storage time. Nevertheless, as deduced from the  
443 moisture equilibration time, CNC seem to slightly reduce WVP values (increase in the  
444 tortuosity factor for mass transfer), but to a very limited extent, probably due to their  
445 high water affinity which contributes to the hydrophilic character of the matrix and to  
446 solubility of water molecules, thus enhancing water transport.

447 Optical properties, UV-VIS spectra, transparency ( $T_i$ ) and gloss of the films are directly  
448 related with their nano- and micro-structure. The UV-VIS spectra of control and  
449 cellulose nanocrystals based films in the UV range are shown in Figure 7, where the  
450 greatest differences were observed. The films exhibit higher values of transmittance ( $T$ )  
451 in the visible light range (400-800 nm) than in the UV range (200-400 nm), according to  
452 Chen et al., [42] for PVA films. The control films exhibited values of transmittance  
453 above 90 % in the visible light range, whereas the values were much lower in the UV  
454 range. The addition of cellulose nanocrystals provoked a decrease in film transmittance  
455 over the whole UV-VIS range, but this is more marked in the UV range, where  $T$  values  
456 decreased by about 60 % for the films with the highest ratio of nanocrystals. These  
457 results confirm the greater opacity to UV radiation of nanocomposites observed by  
458 other authors [10, 20], which represents an advantage in terms of the food protection  
459 against oxidative processes or other UV induced reactions. In terms of transparency to  
460 visible light, the internal transmittance ( $T_i$ ) at 450 nm (Table 2) reveals a small  
461 progressive increase in opacity as the CNC ratio rose in the films, regardless of the  
462 storage time, in agreement with the rise in the concentration of the nanocrystal  
463 dispersed phase. As concerns the film' gloss, they showed very low values at 60°  
464 incidence angle, as compared with the gloss values of pure pea starch or PVA films (27  
465 and 150 units, respectively, data not reported). This can be attributed to the surface  
466 roughness of the films where lumps of the starch-rich phase are dispersed in the  
467 continuous PVA-rich phase, as discussed above. This provoked irregularities at the film  
468 surface which contributes to light dispersion, giving a matt appearance. The  
469 incorporation of CNC did not significantly affect the gloss of the films.

470 The mechanical behaviour of the films is shown in Figure 8 where the typical stress-  
471 strain curves of control blend (C) and CNC composite films 1 %, 3 % and 5 % , after 5  
472 weeks of storage time are shown. The different tensile behaviour of control films and  
473 composites can be clearly observed. The presence of CNC affected the film  
474 extensibility; the higher the CNC ratio, the more stretchable the material. Similar

475 behaviour has been reported by several authors [8, 20] for other films containing CNC.  
476 It is highlighted that the extensible response of films is closely related to the different  
477 concentrations of nanocrystals in the matrix, determining the volume fraction of the  
478 reinforcement, the dispersion degree in the matrix, and the interactions between the  
479 nanocrystals and the polymers [15].

480 Elastic modulus (EM), tensile strength at break (TS) and percentage of elongation at  
481 break ( $\epsilon$  %) are used to describe the mechanical behaviour of films. Table 3 shows the  
482 mean values of these parameters for control films and composites. The obtained  
483 values are coherent with those reported by other authors for pea or corn starch-PVA  
484 films [24, 28, 30]. Cellulose nanocrystals improved the mechanical behaviour of films in  
485 terms of their stretchability, without decreasing their resistance to break ( $p < 0.05$ ), while  
486 the elastic modulus tends to increase slightly. After 5 weeks' storage time, a similar  
487 behaviour was observed for both blend and composite films: the resistance to break is  
488 reduced, as well as the elastic modulus, which can be attributed to the moisture gain of  
489 the films during storage, which makes the network cohesion forces weaker.

490 Nevertheless, at this time, the reinforcement effect of CNC was more evident since the  
491 elastic modulus of composites containing 3 or 5 % CNC was higher.

492 The mechanical impact of CNCs on blend films can be, in part, explained by the  
493 limitation of crystallization of PVA, but also by the formation of a percolating network  
494 within the polymer matrix, as reported by other authors [6]. In this network, the stress is  
495 assumed to be transferred through crystal-crystal interactions and crystal-polymer  
496 matrix interactions [10]. According to Favier et al. [47], the critical percolation volume  
497 fraction (percolation threshold:  $X_c$ ) can be estimated from statistical percolation theory for  
498 cylindrically shaped particles taking into account their aspect ratio ( $A$ ) by the relation:  
499 ( $X_c = 0.7/A$ ). For composite films with CNCs,  $A$  can be estimated as 20 and  $X_c$  is 0.035.

500 So, percolation threshold was reached for all composites and percolation network  
501 formation can explain the enhancement of mechanical behaviour of the films.

502 PVA-starch films containing cellulose nanocrystals were more stretchable and stiffer  
503 with comparable resistance to break than pea starch-PVA films and so, they can be  
504 considered more adequate for food packaging applications.

505 Overall migration tests with simulants were carried out to determine the total amount of  
506 non-volatile substances that might migrate into foodstuffs from film matrices [48] for the  
507 purposes of checking whether they meet the migration limit ( $60 \text{ mg kg}^{-1}$  simulant)  
508 established by current legislation [39]. Table 4 shows the obtained values of overall  
509 migration for control and nanocomposite films in both food simulants. After 20 days in  
510 ethanol 10 % (v/v) simulant, no significant differences in overall migration ( $p \leq 0.05$ )  
511 between control and composite films were found, except for films with 5 % of CNC  
512 which showed higher values, although well below the established limit. However, after  
513 2 days at  $20 \text{ }^\circ\text{C}$  in isooctane, the maximum migration level was reached for the control  
514 films, although migrated amounts are in the order of 1000 times lower than that  
515 obtained in the polar simulants. The different migration behaviour of control and  
516 nanocomposites in the two food simulants reveals the greater hydrophilic nature of  
517 films containing CNC, as reported by Fortunati, et al. [49]. The CNC addition  
518 significantly decreased ( $p < 0.05$ ) the amount of material that migrates to non-polar food  
519 simulants, while increasing the migrated amounts in polar simulants. Therefore, CNC  
520 make the films more adequate for applications in high fat content foods.

521

## 522 **Conclusions**

523 The pea starch-PVA blend films showed phase separation and CNC are distributed in  
524 both, starch rich phase and PVA rich phase. They are present as aggregates of  
525 different sizes depending on their ratio in the film; the higher the ratio, the greater the  
526 aggregates, as deduced from the AFM analysis at surface level. No changes in water  
527 vapor permeability occurred due to the presence of CNC, despite the increase in the  
528 hydrophilic nature of the films revealed by the overall migration values in polar and  
529 non-polar food simulants. Films with CNC became slightly stiffer and more stretchable

530 than control films, while crystallization of PVA was partially inhibited by CNC addition.  
531 The improvements conferred by CNC in mechanical properties of pea starch-PVA  
532 blend films make them more adequate for food applications, especially for high fat  
533 foods, where overall migration values were very low.

534

### 535 **Acknowledgments**

536 The authors acknowledge the financial support from the Spanish Ministerio de  
537 Economía y Competitividad throughout the projects AGL2010-20694 and AGL2013-  
538 42989-R. Amalia Cano also thanks the Spanish Ministerio de Educación, Cultura y  
539 Deporte for the FPU grant and COST-STSM-FA1001-14253 for the financial support  
540 for the collaboration.

541

### 542 **REFERENCES**

543 [1] Armentano I, Dottori M, Fortunati E, Mattioli S, Kenny JM (2010) Biodegradable  
544 polymer matrix nanocomposites for tissue engineering: A review, Polym Degrad and  
545 Stab 95:2126-2146.

546 [2] Fortunati E, Peltzer M, Armentano I, Jiménez A, Kenny JM (2013) Combined effects  
547 of cellulose nanocrystals and silver nanoparticles on the barrier and migration  
548 properties of PLA nano-biocomposites, J Food Eng 118: 117-124.

549 [3] Siracusa V, Rocculi P, Romani S, Rosa MD (2008) Biodegradable polymers for food  
550 packaging: a review, Trends on Food Sci Technol 19: 634-643.

551 [4] Anandjiwala RD (2006) The role of research and development in the global  
552 competitiveness of natural fibre products, Natural Fibres Vision 2020 New Delhi, 8-9  
553 December 2006: 1-15.

554 [5] Chen Y, Liu Ch, Chang PR, Cao X, Anderson DP (2009) Bionanocomposites based  
555 on pea starch and cellulose nanowhiskers hydrolyzed from pea hull fibre: Effect of  
556 hydrolysis time, Carbohydr Polym 76: 607-615.

- 557 [6] Habibi Y, Lucia LA, Rojas OJ (2010) Cellulose Nanocrystals: Chemistry, self-  
558 assembly, and applications, *Chem Rev* 110(6): 3479-3500.
- 559 [7] Lee SY, Mohan DJ, Kang IE, Doh G-H, Lee S, Han SO (2009) Nanocellulose  
560 reinforced PVA composite films: effects of acid treatment and filler loading, *Fibers and*  
561 *Polym* 10: 77-82.
- 562 [8] Zhang W, Yang X, Li C, Liang M, Lu C, Deng Y (2011) Mechanical activation of  
563 cellulose and its thermoplastic polyvinyl alcohol composites with enhanced  
564 physicochemical properties, *Carbohydr Polym* 83: 257-263.
- 565 [9] Fortunati E, Armentano I, Zhou Q, Iannoni A, Saino E, Visai L, Berglund LA, Kenny  
566 JM (2012) Multifunctional bionanocomposite films of poly(lactic acid), cellulose  
567 nanocrystals and silver nanoparticles, *Carbohydr Polym* 87: 1596-1605.
- 568 [10] Fortunati E, Puglia D, Luzi F, Santulli C, Kenny JM, Torre L (2013) Binary PVA bio-  
569 nanocomposites containing cellulose nanocrystals extracted from different natural  
570 sources: Part I, *Carbohydr Polym* 97: 825-836.
- 571 [11] Cavaille JY, Ruiz MM, Dufrense A, Gerard JF, Graillat C (2000) Processing and  
572 characterization of new thermoset nanocomposites based in cellulose whiskers,  
573 *Compos Interface* 7(2): 117-131.
- 574 [12] Khoshkava V and Kamal MR (2014) Effect of drying conditions on cellulose  
575 nanocrystals (CNC) agglomerate porosity and dispersibility in polymer  
576 nanocomposites, *Powder Technol* 261: 288-298.
- 577 [13] Sturcová A, Davies GR, Eichhorn SJ (2005) Elastic modulus and stress-transfer  
578 properties of tunicate cellulose whiskers, *Biomacromolecules* 6: 1055-1061.
- 579 [14] Fortunati E, Armentano I, Zhou Q, Puglia D, Terenzi A, Berglund LA, Kenny JM  
580 (2012) Microstructure and nanoisothermal cold crystallization of PLA composites based  
581 on silver nanoparticles and nanocrystalline cellulose, *Polym Degrad Stab* 97: 2027-  
582 2036.

583 [15] Rescignano N, Fortunati E, Montesano S, Emilianini C, Kenny JM, Martino S,  
584 Armentano I (2014) PVA bio-nanocomposites: A new take-off using cellulose  
585 nanocrystals and PLGA nanoparticles, *Carbohydr Polym* 99: 47-58.

586 [16] Siqueira G, Brasa J, Follain N, Belbekhouche S, Marais S, Dufresne A (2013)  
587 Thermal and mechanical properties of bio-nanocomposites reinforced by Luffa  
588 cylindrical cellulose nanocrystals, *Carbohydr Polym* 91(2): 711-717.

589 [17] Choi Y and Simonsen J (2006) Cellulose nanocrystals-filled carboxymethyl  
590 cellulose nanocomposites, *J Nanosci Nanocomposites* 6(3): 633-639.

591 [18] Pereda M, Dufresne A, Aranguren MI, Marcovich E (2014) Polyelectrolyte films  
592 based on chitosan/olive oil and reinforced with cellulose nanocrystals, *Carbohydr*  
593 *Polym* 101: 1013-1026.

594 [19] Ma X, Chang PR, Yu J (2008) Properties of biodegradable thermoplastic pea  
595 starch/carboxymethyl cellulose and pea starch/microcrystalline cellulose composites,  
596 *Carbohydr Polym* 72: 369-375.

597 [20] Arrieta M, Fortunati E, Dominici F, Rayón E, Lopez J, Kenny JM (2014a) PLA-  
598 PHB/cellulose based films: mechanical, barrier and disintegration properties,  
599 *Carbohydr Polym* 107: 139-149.

600 [21] Arrieta M, Fortunati E, Dominici F, Rayón E, Lopez J, Kenny JM (2014)  
601 Multifunctional PLA-PHB/cellulose nanocrystals films: processing, structural and  
602 thermal behavior, *Carbohydr Polym* 107: 16-24.

603 [22] Jiménez A, Fabra MJ, Talens P, Chiralt A (2012) Influence of  
604 hydroxypropylmethylcellulose addition and homogenization conditions on properties  
605 and ageing of corn starch based films, *Carbohydr Polym* 89(2): 676-686.

606 [23] Bonilla J, Atarés L, Vargas M, Chiralt A (2013) Properties of wheat starch film-  
607 forming dispersions and films as affected by chitosan addition, *Journal of Food*  
608 *Engineering* 114 (3): 303-312.



609 [24] Cano A, Fortunati E, Cháfer M, Kenny JM, Chiralt A, González C (2015) Properties  
610 and ageing behavior of pea starch films as affected by blend with poly(vinyl alcohol),  
611 Food Hydrocoll 48: 84-93.

612 [25] Siddaramaiah Raj B and Somashekar R (2004) Structure–property relation in  
613 polyvinyl alcohol/starch composites, J Appl Polym Sci 9: 630–635.

614 [26] Priya B, Gupta VK, Pathania D, Singh AS (2014) Synthesis, characterization and  
615 antibacterial activity of biodegradable starch/PVA composite films reinforced with  
616 cellulosic fibre, Carbohydr Polym 109: 171-179.

617 [27] Luo X, Li J, Lin X, (2012). Effect of gelatinization and additives on morphology and  
618 thermal behaviour of cornstarch/PVA blend films, Carbohydr Polym 90: 1595-1600.

619 [28] Shi R, Bi J, Zhang Z, Zhu A, Chen D, Zhou X, Zhang L, Tian W (2008) The effect  
620 of citric acid on the structural properties and cytotoxicity of the polyvinylalcohol/starch  
621 films when molding at high temperature, Carbohydr Polym, 74: 763–770.

622 [29] Jiang X, Jiang T, Gan L, Zhang X, Dai H, Zhang X (2012) The plasticizing  
623 mechanism and effect of calcium chloride on starch/poly(vinyl alcohol) films, Carbohydr  
624 Polym 90: 1677-1684.

625 [30] Yoon S, Park M, Byun H (2012) Mechanical and water barrier properties of  
626 starch/PVA composite films by adding nano-sized poly(methylmethacrylate-co-  
627 acrylamide) particles, Carbohydr Polym 87: 676– 686.

628 [31] Cranston ED and Gray DG (2006) Morphological and optical characterization of  
629 polyelectrolyte multilayers incorporating nanocrystalline cellulose, Biomacromolecules  
630 7: 2522–2530.

631 [32] UNE-EN ISO (2008) Paper, board and pulps - Determination of dry matter content  
632 -Oven-drying method, Vol 638.

633 [33] Jiménez A, Fabra MJ, Talens P, Chiralt A (2012). Effect of re-crystallization on  
634 tensile, optical and water vapour barrier properties of corn starch films containing fatty  
635 acids, Food Hydrocoll 26: 302-310.

636 [34] Roohani M, Habibi Y, Belgacem NM, Ebrahim G, NaghiKarimi A, Dufresne A  
637 (2008) Cellulose whiskers reinforced polyvinyl alcohol copolymers Nanocomposites,  
638 European Polym J 44: 2489–2498.

639 [35] ASTM (1995) Standard test methods for water vapour transmission of materials.  
640 Standard designations: E96-95 Annual book of ASTM standards, Philadelphia PA:  
641 American Society for Testing and Materials, 406 - 413.

642 [36] Cano A, Jiménez A, Cháfer M, González C, Chiralt A (2014) Effect of amylose:  
643 amylopectin ratio and rice bran addition on starch films properties, Carbohydr Polym  
644 111: 543-555.

645 [37] UNE-ISO 527-1 (2012) Plastics e determination of tensile properties e Part 1:  
646 General principles.

647 [38] ASTM (1999) Standard test methods for specular gloss. Designation (D523). In  
648 Annual book of ASTM standards, Vol. 06.01. Philadelphia, PA: American Society for  
649 Testing and Materials.

650 [39] European Standard EN 1186-1:2002 Materials and articles in contact with  
651 foodstuffs. Plastics. Guide to the selection of conditions and test methods for overall  
652 migration.

653 [40] Commission Regulation (EU) No 10/2011 of 14 January 2011 on plastic materials  
654 and articles intended to come into contact with food.

655 [41] Sreekumar PA, Al-Harhi MA, De SK (2012) Studies on compatibility of  
656 biodegradable starch/polyvinyl alcohol blends, Polym Engineering Sci 52(10): 2167-  
657 2172.

658 [42] Chen J, Liu Ch, Chen Y, Chen Y, Chang PR (2008) Comparative study on the  
659 films of poly(vinyl alcohol)/pea starch nanocrystals and poly(vinyl alcohol)/native pea  
660 starch, Carbohydr Polym 73: 8-17.

661 [43] Jiménez A, Sánchez-González L, Desorby S, Chiralt A, Tehrani EA (2013)  
662 Influence of nanoliposomes incorporation on properties of film forming dispersions and  
663 films based on corn starch and sodium caseinate, Food Hydrocoll 35: 159-169.

664 [44] Jagadish RS and Raj B (2011) Properties and sorption studies of polyethylene  
665 oxide-starch blended films, *Food Hydrocoll* 25: 1572-1580.

666 [45] Abdelrazek EM, Elashmawi IS, Labeeb S (2010) Chitosan filler effects on the  
667 experimental characterization, spectroscopic investigation and thermal studies of  
668 PVA/PVP blend films, *Physica B*, 405: 2021-2027.

669 [46] Peresin MS, Habibi Y, Zoppe JO, Pawlak JJ, Rojas OJ (2010) Nanofiber  
670 composites of polyvinyl alcohol and cellulose nanocrystals: manufacture and  
671 characterization, *Biomacromolecules* 11(3): 674-681.

672 [47] Favier V, Cavaillé JY, Canova GR, Shrivastavas SC (1997) Mechanical percolation  
673 in cellulose whisker nanocomposites, *Polym Engineering Sci* 37(10): 1732-1739.

674 [48] Schmidt B, Katiyar V, Plackett D, Larsen EH, Gerds N, Bender Koch C (2011)  
675 Migration of nanosized layered double hydroxide platelets from polylactide  
676 nanocomposite films, *Food Addit and Contamin* 28: 956–966.

677 [49] Fortunati E, Peltzer M, Armentano I, Torre L, Jiménez A, Kenny JM (2012) Effects  
678 of modified cellulose nanocrystals on the barrier and migration properties of PLA nano-  
679 biocomposites, *Carbohydr Polym* 90: 948-956.

680 [50] Fortunati E, Puglia D, Monti M, Santulli C, Maniruzzaman M, Kenny JM (2013).  
681 Cellulose nanocrystals extracted from Okra Fibers in PVA nanocomposites. *J Appl*  
682 *Polym Sci*, 3220-3230, DOI: 10.1002/APP.38524.

Table 1: Thermal properties of control blend films and those containing 1, 3 and 5 %wt of CNC obtained by DSC and TGA analysis. Mean values  $\pm$  standard deviation.

FILMS	Cooling				Heating				TGA analysis
	T <sub>c1</sub> (°C)	T <sub>c2</sub> (°C)	$\Delta H_c$ (J.g <sup>-1</sup> <sub>pva</sub> )	T <sub>g</sub> (°C)	T <sub>m</sub> (°C)	$\Delta H_m$ (J.g <sup>-1</sup> <sub>pva</sub> )	X (%)	T <sub>mp</sub> (°C)	T <sub>p</sub> (°C)
<b>C</b>	143.8 $\pm$ 0.9 <sup>a</sup>	200.7 $\pm$ 0.1 <sup>a</sup>	65 $\pm$ 6 <sup>a</sup>	78.6 $\pm$ 0.2 <sup>a</sup>	227.04 $\pm$ 1.12 <sup>a</sup>	108 $\pm$ 6 <sup>a</sup>	67 $\pm$ 4 <sup>a</sup>	347.3 $\pm$ 0.4 <sup>a</sup>	419 $\pm$ 2 <sup>a</sup>
<b>1 %</b>	135 $\pm$ 4 <sup>a</sup>	201.1 $\pm$ 1.2 <sup>a</sup>	74 $\pm$ 8 <sup>a</sup>	76.4 $\pm$ 0.2 <sup>a</sup> <sup>b</sup>	226.8 $\pm$ 0.9 <sup>a</sup>	85 $\pm$ 2 <sup>b</sup>	53 $\pm$ 1 <sup>b</sup>	356 $\pm$ 6 <sup>a</sup>	429 $\pm$ 3 <sup>b</sup>
<b>3 %</b>	141 $\pm$ 3 <sup>b</sup>	201.2 $\pm$ 1.2 <sup>a</sup>	71 $\pm$ 6 <sup>a</sup>	73.9 $\pm$ 1.4 <sup>b</sup>	225.8 $\pm$ 1.8 <sup>a</sup>	85 $\pm$ 3 <sup>b</sup>	53 $\pm$ 2 <sup>b</sup>	355 $\pm$ 2 <sup>a</sup>	431.9 $\pm$ 1.3 <sup>b</sup>
<b>5 %</b>	145.9 $\pm$ 0.1 <sup>ab</sup>	202.3 $\pm$ 0.2 <sup>a</sup>	60.7 $\pm$ 0.2 <sup>a</sup>	76.3 $\pm$ 1.8 <sup>ab</sup>	225.6 $\pm$ 0.7 <sup>a</sup>	61 $\pm$ 6 <sup>c</sup>	38 $\pm$ 4 <sup>c</sup>	323 $\pm$ 5 <sup>b</sup>	427 $\pm$ 2 <sup>b</sup>

T<sub>c</sub>: crystallization temperature; T<sub>m</sub>: melting temperature; T<sub>g</sub>: glass transition temperature;  $\Delta H_c$ : enthalpies of crystallization;  $\Delta H_m$ : enthalpies of melting, X: percentage of crystallinity; T<sub>mp</sub>: main peak temperature and T<sub>p</sub>: temperature of second degradation peak.

<sup>a,b</sup> different letters in the same column indicate significant differences among formulations (p<0.05).

Table 2: Moisture content (MC), water vapour permeability (WVP), internal transmittance (Ti) at 450 nm and gloss values at 60° of control films and those containing 1 %, 3 % and 5 % of CNC, after 1 (1W) and 5 (5W) storage weeks. Mean values ± standard deviation.

FILMS	MC (%d.b.)		WVP (g.mm.kPa <sup>-1</sup> h <sup>-1</sup> m <sup>-2</sup> )		Ti (450nm)		Gloss 60°	
	1W	5W	1W	5W	1W	5W	1W	5W
<b>C</b>	6.6±0.8 <sup>a1</sup>	6.7±0.3 <sup>ab1</sup>	3.5±0.3 <sup>a1</sup>	3.41±0.15 <sup>a1</sup>	18±3 <sup>ab1</sup>	20±3 <sup>a1</sup>	3.5±0.3 <sup>a1</sup>	3.41±0.15 <sup>a1</sup>
<b>1 %</b>	6.4±0.5 <sup>b1</sup>	6.9±0.2 <sup>a1</sup>	3.4±0.3 <sup>a1</sup>	3.6±0.3 <sup>a1</sup>	21±3 <sup>a1</sup>	24±3 <sup>b1</sup>	3.4±0.3 <sup>a1</sup>	3.6±0.3 <sup>a1</sup>
<b>3 %</b>	4.73±0.07 <sup>c1</sup>	6.5±0.3 <sup>b2</sup>	3.43±0.15 <sup>a1</sup>	3.25±0.14 <sup>a1</sup>	15±4 <sup>bc1</sup>	21±3 <sup>a2</sup>	3.43±0.15 <sup>a1</sup>	3.25±0.14 <sup>a1</sup>
<b>5 %</b>	4.5±0.2 <sup>c1</sup>	5.8±0.2 <sup>c2</sup>	3.2±0.3 <sup>a1</sup>	3.07±0.66 <sup>a1</sup>	13±4 <sup>c1</sup>	16±3 <sup>c1</sup>	3.2±0.3 <sup>a1</sup>	3.1±0.6 <sup>a1</sup>

<sup>a,b,c</sup> different letter in the same column indicate significant differences among formulations (p<0.05).

<sup>1,2</sup> different number in the same file indicate significant differences among storage time (p<0.05).

Table 3: Values of elastic modulus (EM), tensile strength at break (TS) and percentage of elongation at break ( $\epsilon$ , %) of control blend films and those containing 1 %, 3 % and 5 % of CNC, after 1 (1W) and 5 (5W) storage weeks. Mean values  $\pm$  standard deviation.

FILMS	EM (MPa)		TS (MPa)		$\epsilon$ (%)	
	1W	5W	1W	5W	1W	5W
<b>C</b>	420 $\pm$ 90 <sup>a1</sup>	330 $\pm$ 130 <sup>a1</sup>	19 $\pm$ 5 <sup>a1</sup>	13 $\pm$ 5 <sup>a2</sup>	90 $\pm$ 30 <sup>ab1</sup>	120 $\pm$ 90 <sup>ab1</sup>
<b>1 %</b>	590 $\pm$ 110 <sup>b1</sup>	380 $\pm$ 90 <sup>ab2</sup>	23 $\pm$ 4 <sup>a1</sup>	13 $\pm$ 3 <sup>a2</sup>	60 $\pm$ 30 <sup>a1</sup>	90 $\pm$ 50 <sup>a1</sup>
<b>3 %</b>	400 $\pm$ 100 <sup>a1</sup>	450 $\pm$ 100 <sup>bc1</sup>	19 $\pm$ 6 <sup>a1</sup>	13 $\pm$ 3 <sup>a2</sup>	130 $\pm$ 70 <sup>b1</sup>	160 $\pm$ 80 <sup>b1</sup>
<b>5 %</b>	440 $\pm$ 170 <sup>a1</sup>	460 $\pm$ 70 <sup>c1</sup>	19 $\pm$ 5 <sup>a1</sup>	12 $\pm$ 3 <sup>a2</sup>	140 $\pm$ 60 <sup>b1</sup>	170 $\pm$ 40 <sup>b1</sup>

<sup>a,b,c</sup> different letter in the same column indicate significant differences among formulations ( $p < 0.05$ ).

<sup>1,2</sup> different number in the same file indicate significant differences among storage time ( $p < 0.05$ ).

Table 4: The overall migration of control blend films and those containing 1 %, 3 % and 5 % of CNC, in 10% (v/v) ethanol and isooctane food simulants. Mean values  $\pm$  standard deviation.

<b>FILMS</b>	<b>Ethanol 10% (v/v) (mg/kg simulant)</b>	<b>Isooctane (<math>\mu</math>g/kg simulant)</b>
<b>C</b>	4.6 $\pm$ 0.7 <sup>a</sup>	34 $\pm$ 3 <sup>a</sup>
<b>1%</b>	4.5 $\pm$ 0.2 <sup>ab</sup>	22 $\pm$ 2 <sup>b</sup>
<b>3%</b>	4.8 $\pm$ 0.2 <sup>ab</sup>	12 $\pm$ 3 <sup>c</sup>
<b>5%</b>	5.8 $\pm$ 1.5 <sup>b</sup>	15 $\pm$ 2 <sup>c</sup>

<sup>a,b</sup> different letter in the same column indicate significant differences among formulations ( $p < 0.05$ ).

## **FIGURE CAPTIONS**

**Figure 1:** FESEM micrographs of the surface of control blend and composite films with different contents of CNC (samples 1 %, 3 % and 5 %).

**Figure 2:** FESEM micrographs of the cross section of control blend and composite films with CNC contents (samples 1 %, 3 % and 5 %). Higher magnification images from top and bottom of the films are included to observe the different separated phases.

**Figure 3:** Phase imaging AFM maps of surface of control blend and composite films with different CNC contents (1 %, 3 % and 5 %). Higher magnification for continuous (CP) and dispersed (DP) phases at the film surface.

**Figure 4:** Maps of Log DTM modulus obtained from AFM in surface of control blend and composite films with different contents of CNC.

**Figure 5:** FTIR spectra of control blend and composite films with different amounts of CNC (1 %, 3 % and 5 %).

**Figure 6:** TG (a) and DTG (b) curves obtained from TGA of control blend and composite films with CNCs (1 %, 3 % and 5 %).

**Figure 7:** Spectral distribution in the UV range of the UV-VIS spectra of control blend (C) and composite films with CNC (1 %, 3 % and 5 %).

**Figure 8:** Typical strain-stress curves of control blend (C) and composite films with CNCs (1 %, 3 % and 5 %) after 5 weeks of storage.



Figure 1.

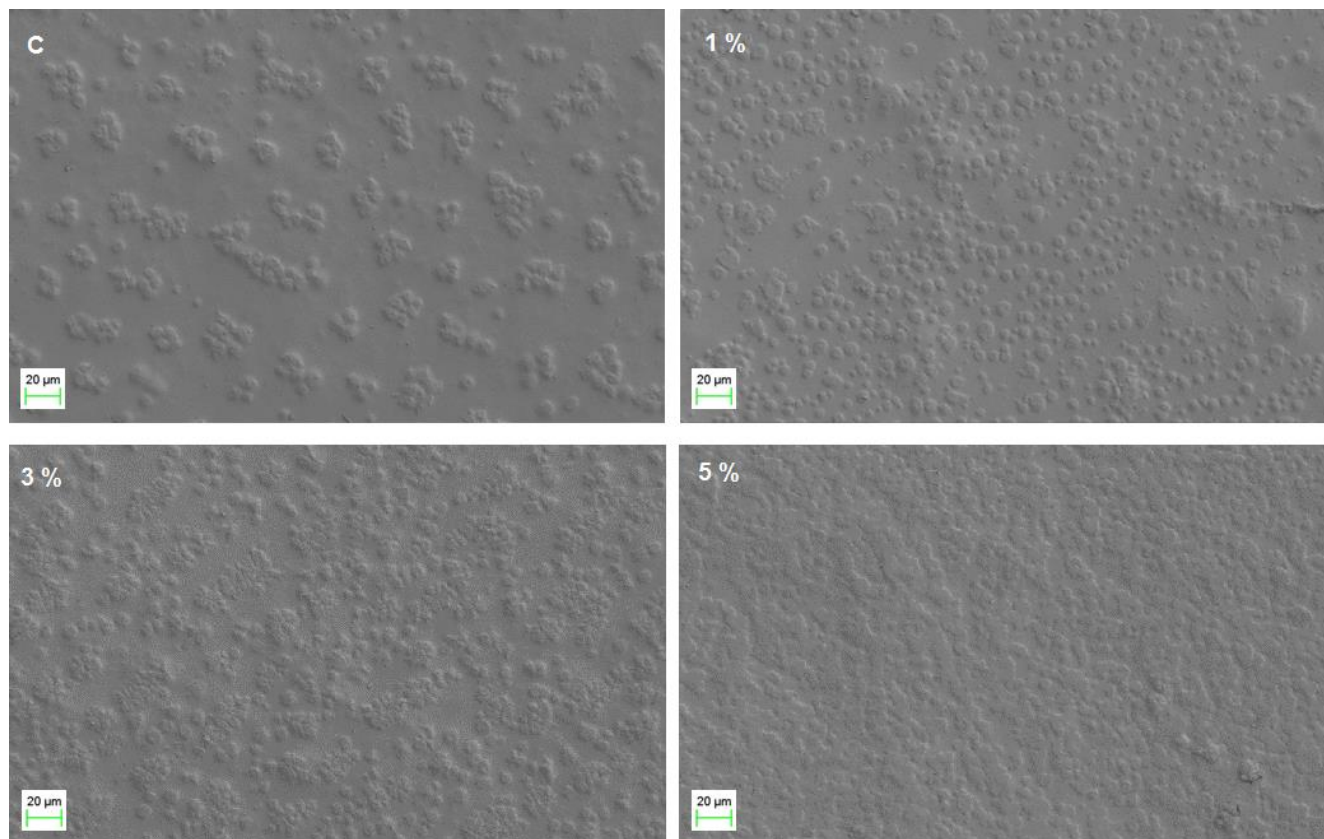


Figure 2.

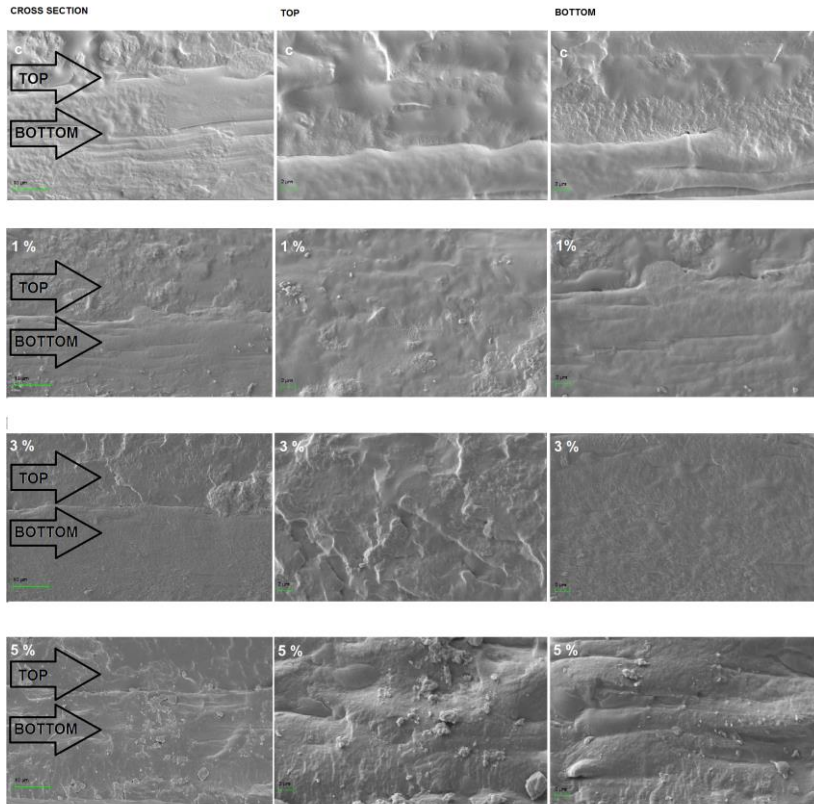




Figure 3.

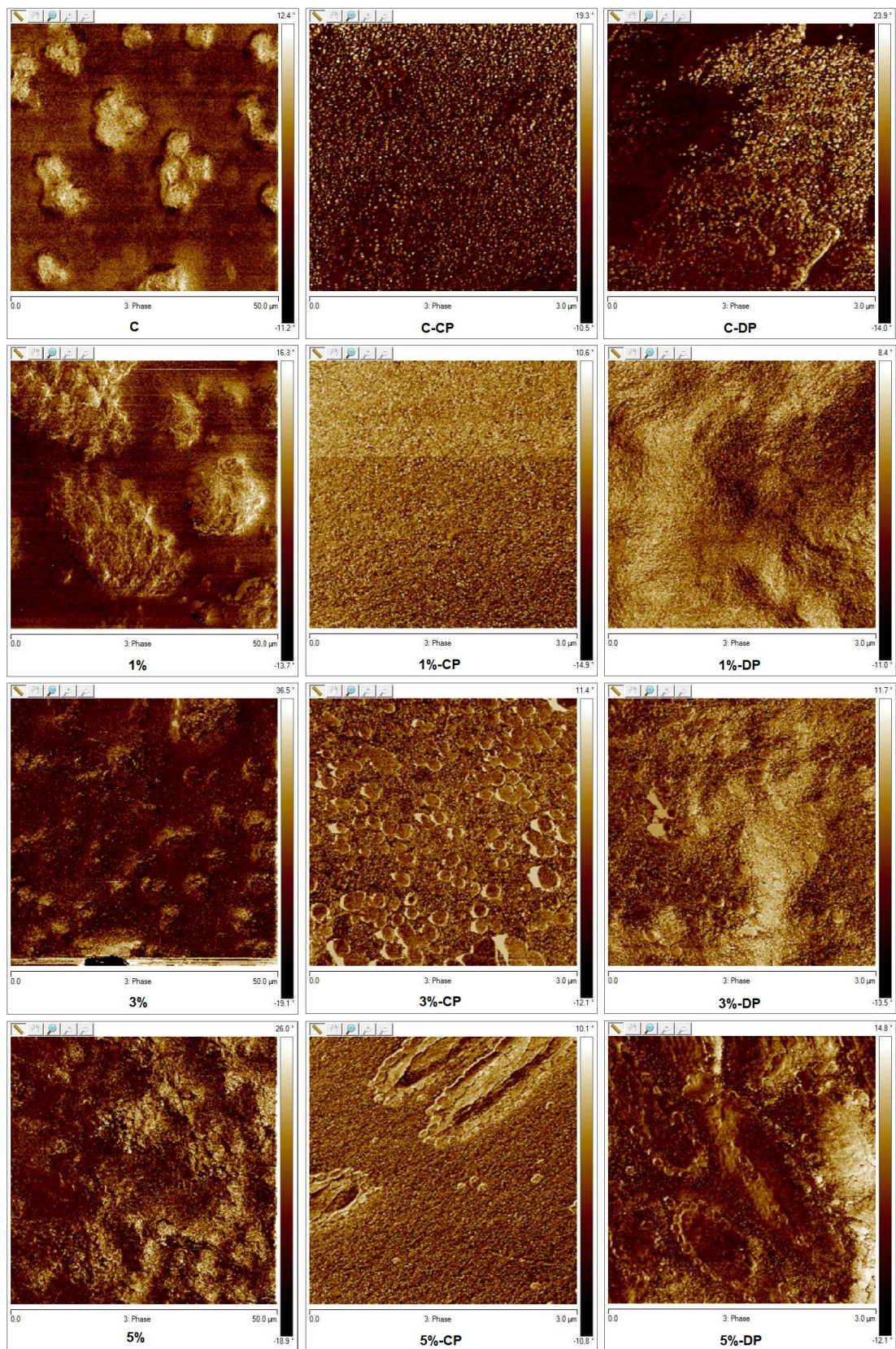




Figure 4.

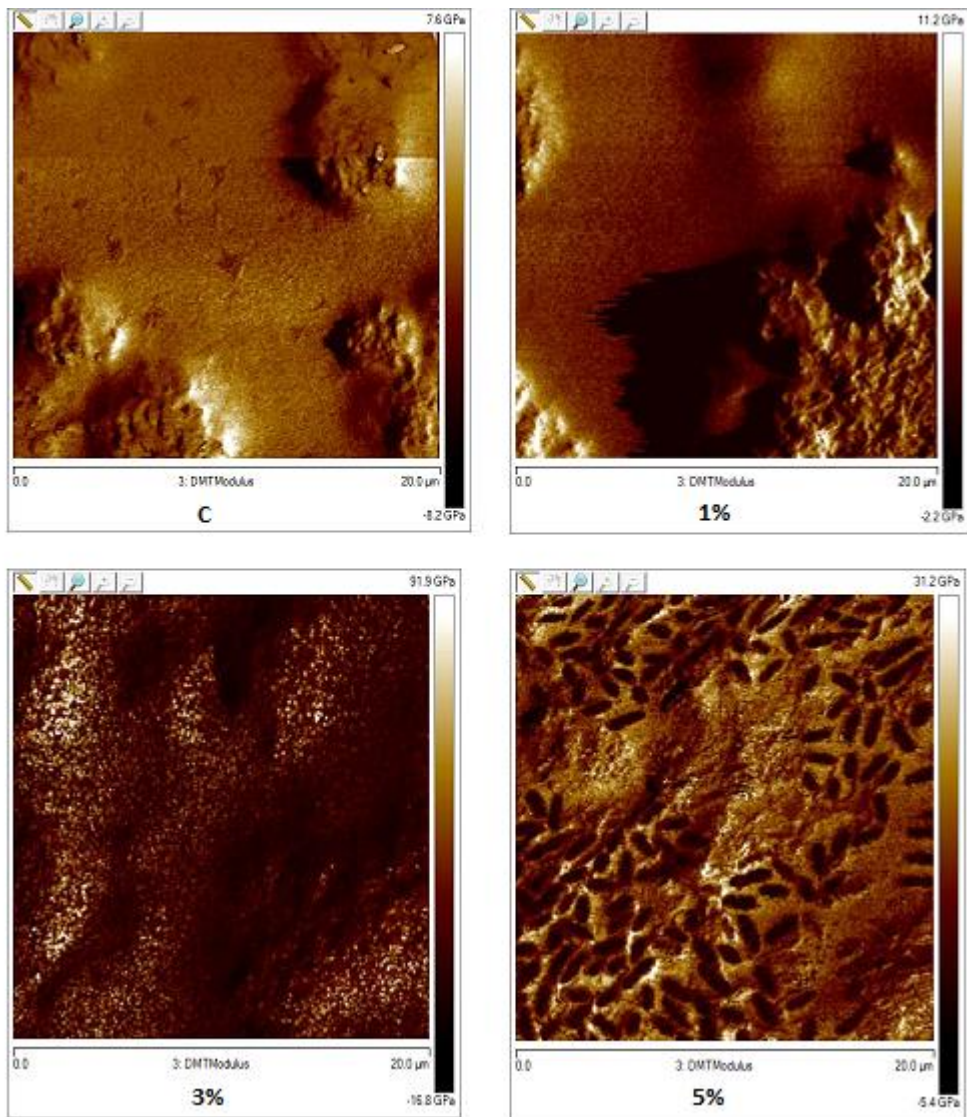


Figure 5.

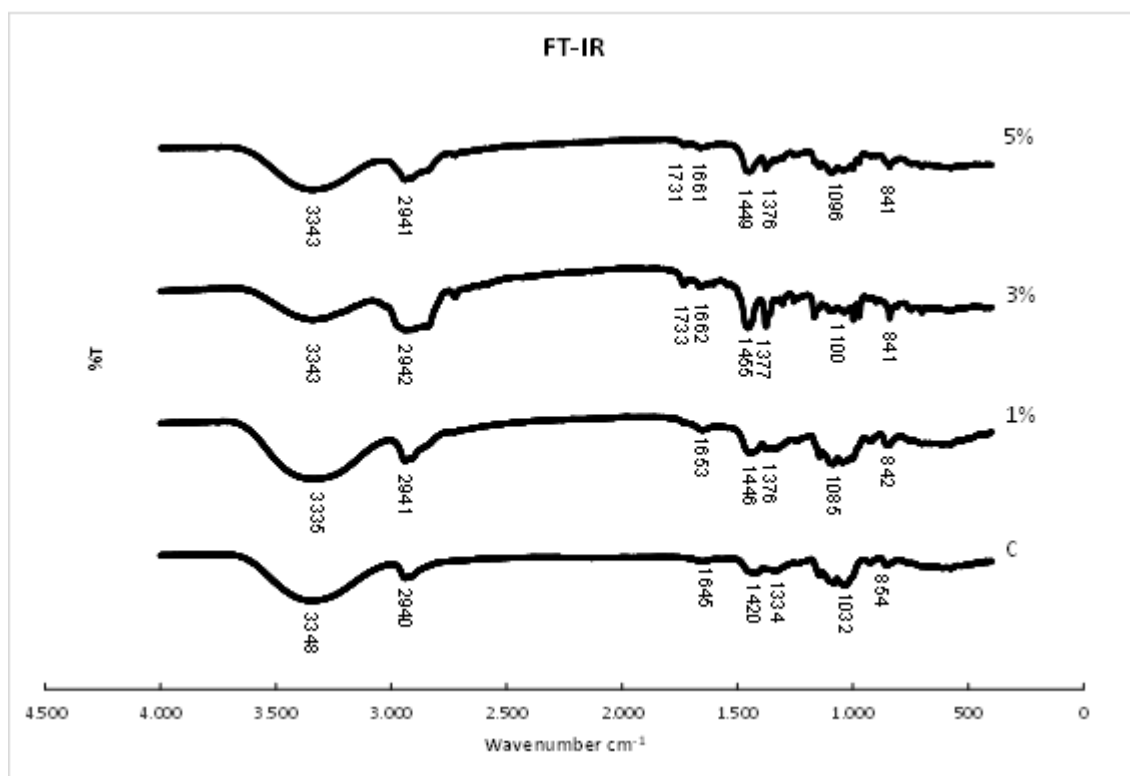


Figure 6.

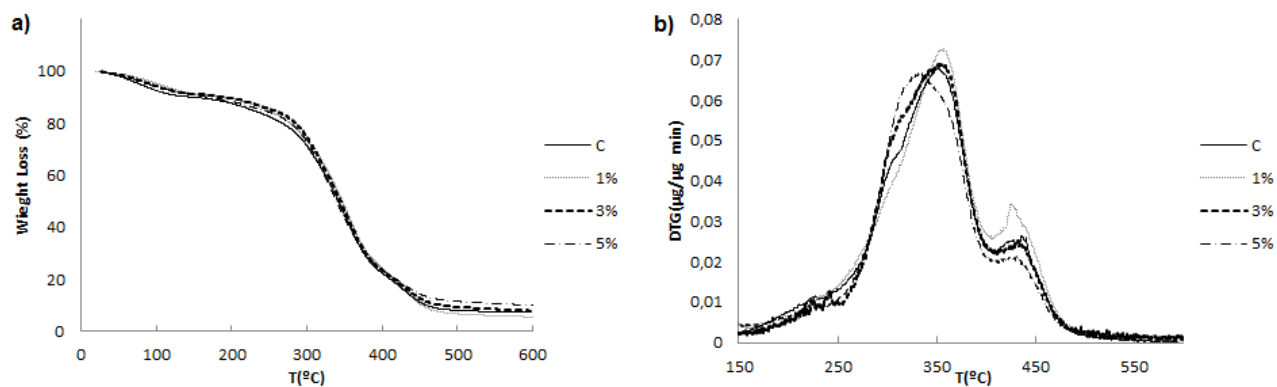


Figure 7.

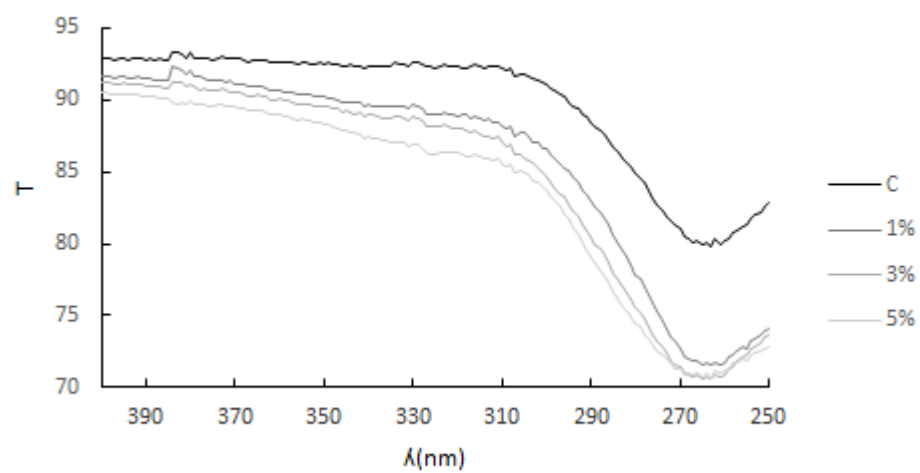


Figure 8.

